Applied Thermal Engineering 206 (2022) 118109

Contents lists available at ScienceDirect

Applied Thermal Engineering

journal homepage: www.elsevier.com/locate/apthermeng

Research Paper

Numerical investigation of the heat transfer characteristics of propane/air flames impinging on a cylindrical surface

Sérgio Cavaleiro Costa, Isabel Malico *

Universidade de Évora, Escola de Ciências e Tecnologia, Rua Romão Ramalho 59, 7000-671 Évora, Portugal
LAETA, IDMEC, Instituto Superior Técnico, Universidade de Lisboa, Av. Rovisco Pais 1, 1049-001 Lisboa, Portugal

ARTICLE INFO

Keywords:
Furnace
Direct flame impingement
Convex cylindrical target
Combustion
Computational Fluid Dynamics (CFD)
Nusselt number

ABSTRACT

To better understand the complex phenomena occurring inside furnaces with direct flame impingement and extend the existent studies to situations with multiple enclosed jets, numerical simulations of a radial array of four turbulent confined flame jets impinging on a cylinder are presented. The three-dimensional, incompressible, steady, averaged equations for the transport of mass, momentum, energy and species were solved. Turbulence was modeled with the realizable k-ε model, combustion with the finite-rate/eddy-dissipation model and radiation with the finite-volume scheme. The reference condition simulated is based on the operation of an existent industrial furnace, but the Reynolds number, excess air ratio, impinging distance, cylindrical target diameter and reactant temperature were varied in order to analyze their influence on the fluid flow and heat transfer and to determine a correlation for the area-averaged Nusselt number. The curvature of the target and the interaction of adjacent opposed wall jets lead to the increase of the heat transfer to the target. For the parameter values considered, the excess air ratio, Reynolds number and reactant temperature are of primary importance to enhance heat transfer and reduce the power required, while the target curvature is of secondary importance and the least influential parameter is the impinging distance.

1. Introduction

Optimization of the heating processes in the metal industry is becoming more important with the increased pressure for the industry to improve efficiency and reduce emissions. The diversity of equipment that generates process heat in the metal industry is large. Among them, multiple-zone gas fired furnaces with direct flame impingement are established in the market for heating billets prior to extrusion. These furnaces are composed of a large array of burners with their axis placed normal to the load and configured to impinge the combustion jets directly onto the surface of the billet. As a consequence of the flame-wall interaction, they present higher heating rates and efficiencies than conventional furnaces, thereby reducing energy consumption [1,2]. When the billet has a circular cross-section, the flame impinges on a convex curved surface, resulting in a complex, three-dimensional reactive flow.

The number of studies that focus on flame impinging on curved surfaces is very limited [3,4], but these efforts are of utmost importance for the understanding of the phenomena that occur inside furnaces with direct-flame impingement. The first comprehensive study of the heat transfer characteristics of a laminar premixed flame impinging on a cylindrical surface can be attributed to Chander and Ray [5], who experimentally studied the effects on the heat transfer characteristics of varying the Reynolds number, equivalence ratio, separation distance and burner diameter to cylinder diameter ratio and developed correlations for stagnation point heat flux. The authors concluded that, compared to flat plates, flames impinging on a cylindrical surface produce higher stagnation region heat fluxes, but that trend is reversed in the wall-jet region. Yousefi-Asli et al. [6] experimentally obtained the Nusselt number and temperature field of laminar methane/air premixed flames impinging on a cylindrical surface and studied the effects of the same operating conditions. In their work, the burner is rectangular and not circular. Oketch et al. [4,7] measured the stagnation point heat flux of laminar premixed methane/air flame impinging on an aluminum cylinder. The authors discussed the flame stabilization mechanism as a function of the burner velocity relative to the laminar flame speed and the effects of changing the equivalence ratio and the separation distance. Kuntikana and Prabhu [8] focused on the characterization of single laminar methane/air premixed flames jet impinging on both convex and concave surfaces. The authors discussed the effect of varying several

* Corresponding author.
E-mail address: imbm@uevora.pt (I. Malico).

https://doi.org/10.1016/j.applthermaleng.2022.118109
Received 12 September 2021; Received in revised form 14 December 2021; Accepted 14 January 2022
Available online 20 January 2022
1359-4311/© 2022 Elsevier Ltd. All rights reserved.

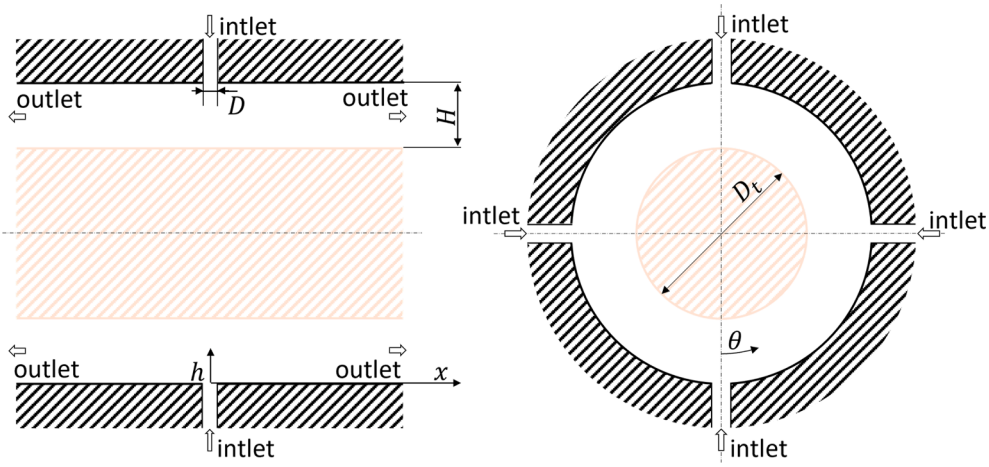

Fig. 1. Simplified geometrical model of one zone of a gas-fired furnace with direct flame impingement.

parameters and concluded that, for the range of conditions studied, the results are more sensitive to variations in the Reynolds number or burner to plate distance than in the equivalence ratio or burner diameter to target diameter ratio. Additionally, the thermal efficiency and average heat flux to the impingement surface are higher for the concave target compared with the convex.

According to what has been said, there are few publications on premixed flames impinging on curved surfaces and, from these, to the best of the authors' knowledge, no comprehensive numerical study exists (most of the studies are experimental). All the studies referred in the above paragraph focus on laminar flames reaching Reynolds numbers up to 1500. As an example of the rarer studies for higher Reynolds numbers, Hargrave et al. [9] measured stagnation point heat fluxes for premixed turbulent methane air jet flames impinging on curved surfaces and compared the results with theoretical predictions; the latter for the case where the target is downstream of the reaction zone. Another characteristic of the studies referred in the above paragraph is that they analyzed single flames, but the study of multiple flames and their interaction is important, since they are more commonly used in the industry [10]. In an array configuration, the individual jets can be arranged in several ways (see, for example, the review by [11]) and, depending on the geometric configuration of the array and its surroundings, the jets may interact with each other [12]. The study of the impingement of multiple isothermal jet and their interactions (e.g., [13–16] for cylindrical targets) is much more explored than that of multiple flame jets. Multiple flame jets impingement on flat surfaces has been studied, for example, by [17–20]. The use of several jets enhance heat transfer uniformity by creating several impingement zones, but in certain configurations may complicate fluid distribution [21]. Ref. [17] showed that, compared to a flame single jet impinging on a flat surface, three inline flame jets enhance both stagnation point and maximum heat fluxes, but reduce the heat transfer in the zone where the jets interact, while [19] reported that a triangular array of three jets presented no significant difference in peak heat flux values. From what has been said, extending the study of flame jet interactions to the case of cylindrical targets is relevant.

Another common characteristic of the studies on premixed flames impinging on curved surfaces referred above is that the flow is external. However, when analyzing multiple-zone gas fired furnaces with direct flame impingement, the flow is confined. Lee et al. [22] and Kim et al. [23] studied experimentally the characteristics of confined laminar slot jets, but did not elaborate on the effects of confining the flow. Höser and von Rohr [24] investigated experimentally the effect of confinement on the behaviour of a jet impinging on a flat target and concluded that it enhances the heat transfer to the target when compared to the unconfined case. This enhancement is attributed to the reduction of the entrainment of ambient air in the flame jet, which leads to higher momentum and temperature of the impinging jet. Since the flow confinement impacts on the fluid flow and heat transfer, the extension of the existent studies to understand the underlying phenomena that occur in internal flows with direct flame impingement in cylinders is important to the development of industrial equipment.

Detailed numerical investigations of confined flames impinging on cylindrical surfaces, like the one presented in this paper, are deemed necessary since they allow the understanding of the interdependencies and influence of the relevant parameters on the heat transfer performance of confined impinging flames, contributing to the comprehensive quantification of important parameters under a wide range of operating conditions. Through the use of Computational Fluid Dynamics (CFD) to carry out numerical experiments, correlations can be obtained and used to assist in the design of equipment where flames impinge on curved surfaces. Numerical studies are, therefore, a complement to the existent experiments and contribute to the understanding of the complex, underlying phenomena that occur in gas fired furnaces with direct flame impingement. For this type of equipment, experiments are challenging and cannot be fully relied on if done in an industrial environment. By contributing to the ability of modeling and optimizing gas fired furnaces with direct flame impingement, numerical models promote the development of cleaner and more resilient future energy systems.

The simulation of the interactions between flame jets and between flame jets and the cylindrical load in an enclosed environment under different conditions is a step forward for understanding the complex phenomena that occur inside gas fired furnace with direct flame impingement. Having this in mind, in this study, a radial array of four turbulent confined flame jets impinging on a cylindrical surface is numerically investigated through the use of a CFD model. The geometry considered is part of a larger piece of equipment installed in a real industrial unit. Effects of varying the values of the Reynolds numbers ($\mathrm{Re} \in [4200, 8700]$), equivalence ratio ($\Psi \in [1, 2]$), the ratio between the separation distance to the target and the burner diameter ($H/D \in [3, 6]$), cylindrical target diameter to burner diameter ratio ($D_t/D \in [10, 20]$) and reactant temperature ($T_r \in [450\ \mathrm{K}, 550\ \mathrm{K}]$) on the heat transfer characteristics are investigated. To reach the goals proposed in the paper, it is organized as follows; Section 2 describes the configuration that is studied in this paper; Section 3 presents the model used and Section 4 the results obtained and their analysis; finally, in Section 5, conclusions are drawn.

2. Geometrical model and operation conditions

The geometry analyzed in this work is a simplification of a zone of a gas fired furnace with direct flame impingement operating in an existent

Table 1
Reference values for the parameters. Based on [25].

	D [m]	H [m]	D_t [m]	Re	Ψ	T_r [K]	T_t [K]
Reference values	0.017724	0.0625	0.255	4800	1.8	500	850

extrusion line. This real furnace is 22 m long and includes 78 rows of burners with a total of 312 burners. In it, the distance between the centers of two burners, S, is around 8 times the diameter of each individual burner, D. A simulation of the furnace operating at a specific set of operating conditions was already carried out and the results used for validation of the numerical model presented in this paper [25]. However, modeling the entire furnace introduces high geometric complexity, hampers the use of fine meshes and carrying out comprehensive parametric studies. Therefore, we have decided to analyze a simplified geometric model of only one array of four burners (Fig. 1). By doing this, the possible interactions between the flame jets of each row were not simulated. However, even though there is no study on the impingement on curved targets of flame jets with the arrangement present in the industrial furnace that served as a reference to the present work, the study by [17] puts this simplification into perspective. Dong et al. [17] experimentally investigated an inline arrangement of three impinging flame jets on a flat plate and concluded that the between-jet interference is stronger when the S/D and the H/D (impinging distance to burner diameter) ratios are small. When the S/D ratio tested was seven (below the one of the industrial furnace), between-jet interference was only observed at H/D of two (below the lowest ratio considered in this study). From what was said, we conclude that the simplified geometric model considered in this study allows making detailed parametric simulations and understanding the complex phenomena that occur in a section of the real industrial furnace containing four radial burners that impinge on a curved target.

Fig. 1 shows plane sections (front and side views) of the geometric model considered. The cylindrical target, with a diameter D_t, is represented in the middle of the drawing in pink, and the four burners, with a hydraulic diameter D, are radially placed on the cylindrical wall of the furnace at a distance H to the target surface. The fluid enters the furnace radially, impinges on the target surface, deflects and leaves the domain along the direction of the target axis.

The choice of the reference simulation presented in this paper was based on parameters that are typical of the operation of an industrial furnace operating in a company that produces brass rods [25] (Table 1). In the industrial billet heating furnace that served as the model to this work, the billet has a temperature that increases along the axis of the furnace. In this study, the set point temperature at a zone in the middle of the furnace was taken as the temperature at the surface of the billet, T_t. Also, the reactant temperature, T_r, is the one measured at that zone. The burners of the industrial furnace have a diameter of 20 mm, but in the simplified geometrical model implemented in this work, the burners have a square cross-section with the same cross-sectional area, which results in a hydraulic diameter, D, of 17.724 mm. The impact of this simplification was investigated by comparing the results obtained with both square and circular cross-section burners for the simulation with the reference values for the parameters. The impact of this simplification on the area-averaged Nusselt number was 0.09%, and, therefore considered negligible.

After simulating the reference conditions, relevant parameters were varied in order to understand their influence on the characteristics of the fluid flow, combustion and heat transfer. The separation distance of the burner to the target, H/D, was varied from 3 to 6, while the cylinder diameter ratio to burner diameter, D_t/D, was varied from 10 to 20.

The Reynolds number (defined as $\mathrm{Re} = \frac{\rho V D}{\mu}$, where V is the average velocity at the burner exit and ρ and μ the reactant density and viscosity at the entrance of the furnace, respectively) was varied from 4200 to 8700. The fuel, propane, is premixed with the oxidant, air, and the reactants enter the furnace at a temperature, T_r, which was varied between 450 and 550 K. The excess air coefficients, Ψ, considered ranged from 1.0 to 2.0. A table presenting the parameter values for all the simulations carried out in the present study is given in Table A1 of the Appendix.

3. Mathematical and numerical models

In the gas region, the three-dimensional, incompressible, steady, averaged equations for the transport of mass, momentum, energy and species (Eqs. (1)–(4)) were solved.

$$\frac{\partial(\rho u_j)}{\partial x_j} = 0 \tag{1}$$

$$\frac{\partial(\rho u_j u_i)}{\partial x_j} = -\frac{\partial p}{\partial x_i} + \frac{\partial}{\partial x_j}\left[\mu\left(\frac{\partial u_i}{\partial x_j} + \frac{\partial u_j}{\partial x_i} - \frac{2}{3}\delta_{ij}\frac{\partial u_k}{\partial x_k}\right)\right] + \frac{\partial\left(-\rho\widetilde{u_j' u_i'}\right)}{\partial x_j} \tag{2}$$

$$\frac{\partial(\rho u_j h)}{\partial x_j} = \frac{\partial}{\partial x_j}\left(\left(k + \frac{c_p \mu_t}{Pr_t}\right)\frac{\partial T}{\partial x_j}\right) + S_c - \frac{\partial q_j}{\partial x_j} \tag{3}$$

$$\frac{\partial(\rho u_j Y_i)}{\partial x_j} = \frac{\partial}{\partial x_j}\left(\left(\rho D_{i,m} + \frac{\mu_t}{Sc_t}\right)\frac{\partial Y_i}{\partial x_j}\right) + R_i \tag{4}$$

where ρ is the density, u_j the averaged velocity component in the direction j, x_j the j^{th} coordinate, p the pressure, μ the dynamic viscosity, δ_{ij} the Kronecker symbol, u_j' the fluctuating velocity component in direction j, h the specific sensible enthalpy, k the thermal conductivity, c_p the specific heat capacity, μ_t the turbulent viscosity, Pr_t the turbulent Prandtl number, T the temperature, S_c the volumetric source of energy due to combustion, q_j the j^{th} component of the radiative heat flux vector, Y_i the mass fraction of species i, $D_{i,m}$ the mass diffusion coefficient for species i in the mixture, Sc_t the turbulent Schmidt number and R_i the volumetric rate of production of species i. The dilute approximation was used to describe ordinary mass diffusion and the Soret and Dufour effects were not considered. The gaseous mixture was considered an ideal gas and its properties were determined as a function of the temperature. For ideal gases, the specific sensible enthalpy is defined as

$$h = \sum_i Y_i h_i = \sum_i Y_i \left(\int_{T_{ref}}^{T} c_{p,i} dT\right) \tag{5}$$

where $c_{p,i}$ is the specific heat capacity of species i and $T_{ref} = 298$ K.

The Reynolds stresses, last term in Eq. (2), were modeled with the realizable k-ε turbulence model [26], which uses the Boussinesq hypothesis to relate these stresses to the mean velocity gradient and the turbulent viscosity calculated by Eq. (7) (Eq. (6)).

$$-\rho\widetilde{u_i' u_j'} = \mu_t\left(\frac{\partial u_i}{\partial x_j} + \frac{\partial u_j}{\partial x_i}\right) - \frac{2}{3}\left(\rho k + \mu_t \frac{\partial u_k}{\partial x_k}\right)\delta_{ij} \tag{6}$$

$$\mu_t = C_\mu \rho \frac{k^2}{\varepsilon} \tag{7}$$

In this turbulence model, C_μ is a function of the mean strain and rotation rates and of the turbulence fields (See [26] for details). The transport equations for the turbulent kinetic energy, k, (Eq. (8)) and its dissipation rate, ε, (Eq. (9)) were solved.

$$\frac{\partial(\rho u_j k)}{\partial x_j} = \frac{\partial}{\partial x_j}\left[\left(\mu + \frac{\mu_t}{\sigma_k}\right)\frac{\partial k}{\partial x_j}\right] - \mu_t S^2 - \rho\varepsilon \tag{8}$$

$$\frac{\partial(\rho u_j \varepsilon)}{\partial x_j} = \frac{\partial}{\partial x_j}\left[\left(\mu + \frac{\mu_t}{\sigma_\varepsilon}\right)\frac{\partial \varepsilon}{\partial x_j}\right] - \rho C_1 S\varepsilon - \rho C_2 \frac{\varepsilon^2}{k + \sqrt{\nu\varepsilon}} \tag{9}$$

where ν is the kinematic viscosity, S the modulus of the mean rate-of-train tensor defined as $\sqrt{2S_{ij}S_{ij}}$, $S_{ij} = \left(\partial u_j/\partial x_i + \partial u_i/\partial x_j\right)/2$, $\sigma_k = 1.0$,

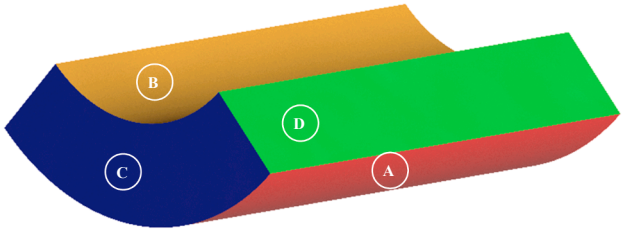

Fig. 2. Computational domain of one-zone of a gas-fired furnace with direct flame impingement.

$\sigma_\varepsilon = 1.2$, $C_2 = 1.9$ and $C_1 = \max[0.43,\eta/(\eta+5)]]$ with η defined as $(Sk)/\varepsilon$.

The premixed combustion of propane and air is modeled as an irreversible, complete reaction, and the rates of production of the chemical species are determined both by Arrhenius reaction rates and mixing rates, the smaller of the two being used (finite-rate/eddy-dissipation model). The finite-rate model neglects the effects of turbulence and for the eddy-dissipation model the overall rate of reaction is controlled by turbulent mixing. The eddy-dissipation turbulence-chemistry interaction model is based on the work of Magnussen and Hjertager [27].

A source term that accounts for thermal radiation is included in the energy conservation equation by solving the radiative transfer equation. The absorption coefficient used is composition-dependent and obtained with the weighted-sum-of-grey-gases model. The interaction between turbulence and radiation is neglected.

A near-wall modeling approach (enhancement wall treatment) was followed, the turbulence model modified and the viscosity-affected near-wall region completely resolved. In this case, the mesh near the wall should be fine enough in the direction normal to the surface to be able to resolve the viscous sublayer. In the present simulation, the average y^+ was 0.1826 and the maximum 1.8199 so that the first node cell from the wall lies within the viscous sublayer.

As far as boundary conditions are concerned, no-slip conditions were imposed at all walls. Solid surfaces are considered diffusely emitting and diffusely reflecting. The furnace interior wall is covered with refractory material with an emissivity of 0.9 and considered adiabatic. The billet (target surface) is considered to have an emissivity of 0.82 [25] and constant temperature (as explained in the previous section). At the gaseous outlets, zero-diffusion flux conditions were imposed. At the burner exit, it was assumed that the flow is uniform and the velocity of the reactants was calculated as a function of the Reynolds number considered for each simulation and of the temperature and composition of the reactants (which is a function of the excess air). The temperature of the reactants was imposed and the turbulence intensity at the burner exit was set to 6%.

By taking advantage of the symmetries that the geometrical model (Fig. 1) presents, the computational domain was reduced to a quarter. The length of the computational domain, L (124D), was large enough to appropriately reduce the influence of the outflow boundary conditions. Fig. 2 shows a view of the computational domain. The letters and color scheme used reflect the different boundary conditions applied (A/red: furnace wall; B/brown: target wall; C/blue: outlet; D/green: symmetry plane). The burner is not visible, but is centered on the furnace wall.

A structured grid with 1 375 000 control volumes was generated when the H/D and D_t/D reference values were considered. For this grid, a maximum volume distortion of 0.08 was achieved with a minimum orthogonality quality of 0.99. A grid independence study was undertaken and the wall shear stress and heat flux to the billet surface were chosen to assess grid convergence. For the reference simulation with the grid of 1 375 thousand control volumes, the area-averaged wall shear stress and the heat flux were predicted within, respectively, 0.3% and 1.3% of the values obtained on the finest grid, which had 1 900 thousand control volumes. For the cases with different burner to target distances or target diameters, other grids had to be generated, but always keeping a similar grid quality. The grids used to obtain the results presented in this paper were considered a good compromise between computational error and computational time.

ANSYS FLUENT 20.0 R2 was used to solve the set of governing equations [28]. The SIMPLEC algorithm was used for the pressure–velocity coupling [29] and the second-order upwind scheme for all spatial discretizations. Radiation through participating media was calculated with the finite-volume scheme [30,31] and the absorption coefficient calculated with the weighted-sum-of-gray-gases model. Radiation was evaluated every ten iterations using first-order upwind and an angular discretization of each octant of the angular space into three polar and three azimuthal angles. The convergence of the solution was achieved when the energy equation residuals dropped below 10^{-7} and there was a guarantee of low mass and energy imbalances when compared to the inlet values (below 0.1%).

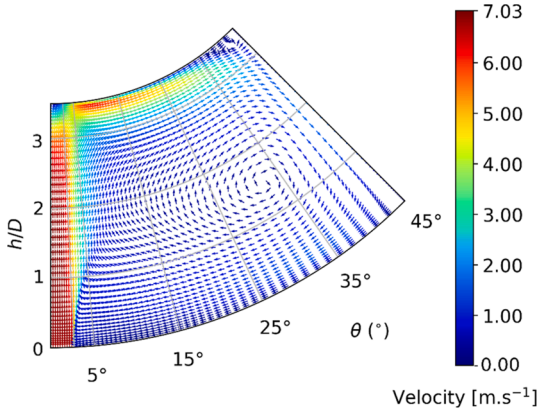

Fig. 4. Velocity vectors in the cross-sectional plane at $x = 0$ for $D_t/D = 14.4$, $H/D = 3.5$, Re = 8700, $\Psi = 1.8$, $T_r = 500$ K and $T_t = 850$ K.

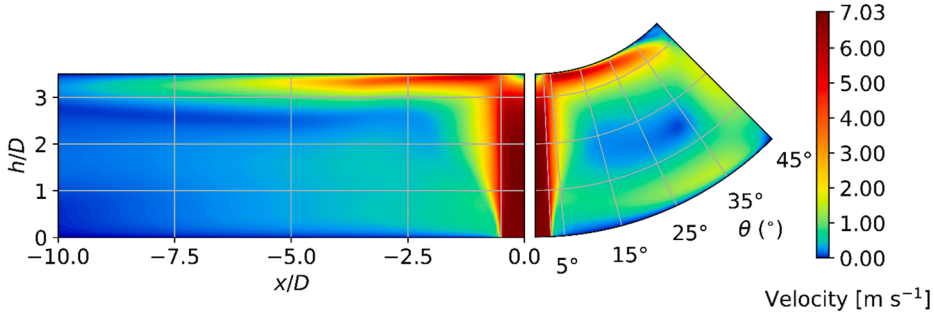

Fig. 3. Velocity field of propane/air impinging on a cylindrical surface at $\theta = 0°$ (left) and $x = 0$ m (right) and with $D_t/D = 14.4$, $H/D = 3.5$, Re = 8700, $\Psi = 1.8$, $T_r = 500$ K and $T_t = 850$ K.

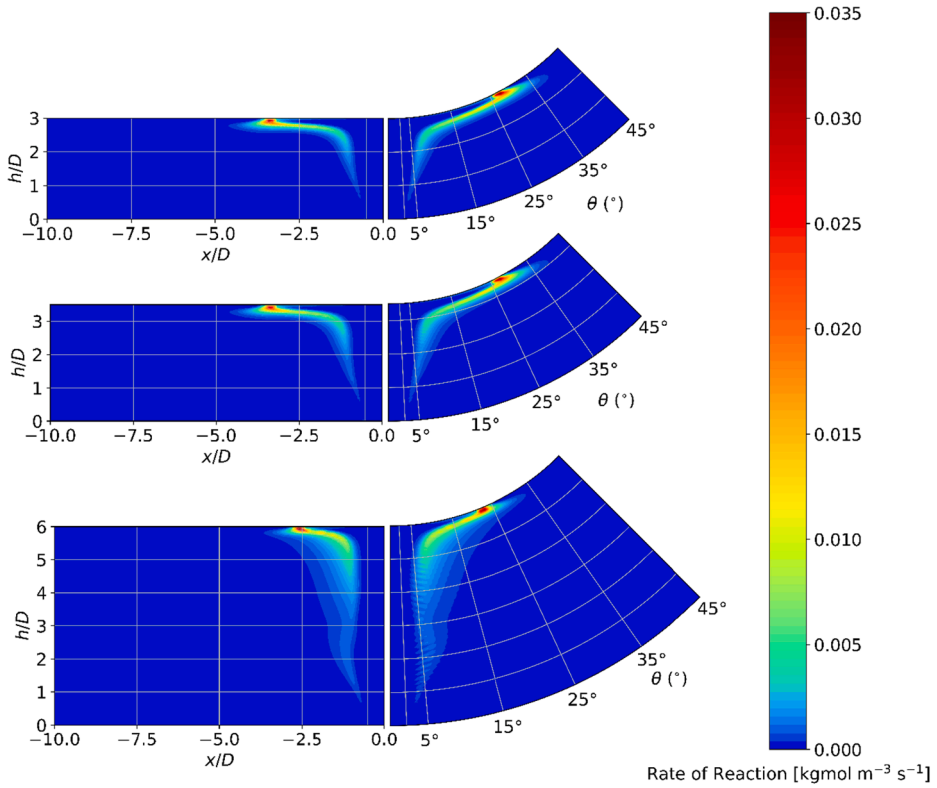

Fig. 5. Reaction rate contour plots of propane/air impinging on a cylindrical surface with $D_t/D = 14.4$, Re = 4800, $\Psi = 1.8$, $T_r = 500$ K, $T_t = 850$ K and H/D equal to 3.0 (top), 3.5 (center), and 6.0 (bottom).

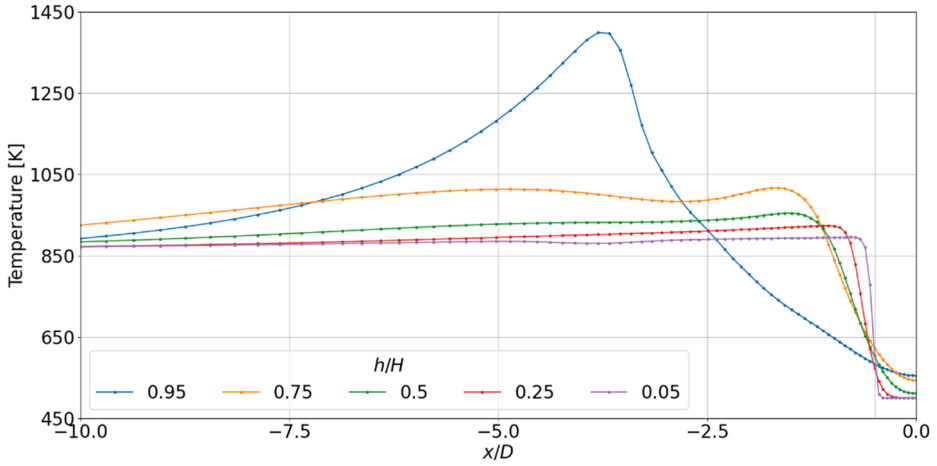

Fig. 6. Fluid temperature in the x/D-direction for propane/air flames impinging on a cylindrical surface with $D_t/D = 14.4$, Re = 4800, $\Psi = 1.8$, $T_r = 500$ K, $T_t = 850$ K, $H/D = 3.5$ and at several heights from the burner.

4. Results and discussion

4.1. Flow configuration

Fig. 3 shows the velocity field contour at two different orthogonal planes that intercept at the axis of the burner, which is placed at $x = 0$ and $\theta = 0°$: on the left, $x/D \in [-10, 0]$, $h/D \in [0, H/D]$ and $\theta = 0°$, and on the right, $x/D = 0$, $h/D \in [0, H/D]$ and $\theta \in [0, 45°]$. The reactants exit the burner at $h = 0$, while the cylindrical target surface is positioned at $h = H$. For reference, the axial and angular position of the burner inner wall is marked in both planes by the gridline closest to the origin (with no label). This figure corresponds to the case where all operating conditions are the reference ones (Table 1) except for the Reynolds number, which is 8700 (the highest Reynolds number simulated). These conditions were chosen because at high Reynolds numbers the flow patterns are more pronounced, but they are generally similar for all cases analyzed.

After the reactants enter the furnace radially to the target axis as a free jet, the gaseous mixture impinges on the target surface, where a stagnation region is clearly visible. In this region, the flow deflects predominantly in the radial direction to the burner axis, becomes mainly tangential to the target wall and accelerates because of the existent favorable pressure gradient. A velocity similar to the inlet jet velocity is attained, but after this point, the flow starts to decelerate again. The deceleration visible on the plane $\theta = 0°$ (left) is a result of the influence of the lower and upper shear layers of the wall jet flow. The deceleration

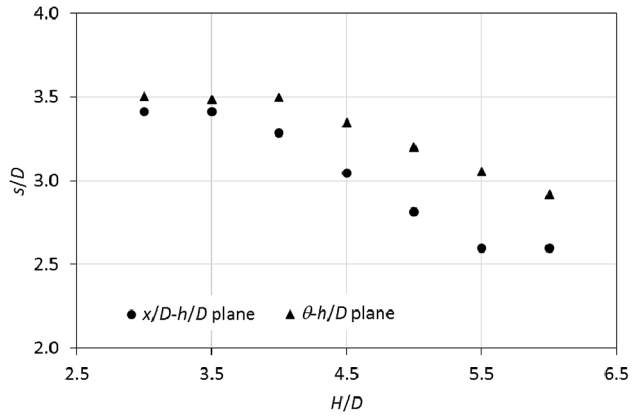

Fig. 7. Distance of the maximum reaction rate to the burner axis vs. H/D for propane/air flames impinging on a cylindrical surface with $D_t/D = 14.4$, Re = 4800, $\Psi = 1.8$, $T_r = 500$ K, $T_t = 850$ K at two different planes. At the plane x/D-h/D with $\theta = 0°$, $s/D = x/D$ and at the plane θ-h/D with $x = 0$, $s/D = \pi(D_t/2 + H\text{-}h)\theta/180$.

visible on the plane $x = 0$ (right) is also a result of the adverse pressure gradient originated by the collision of two adjacent opposed wall jets (only one is shown in Fig. 3, but, as described before, four burners, placed on this cross-sectional plane, 90° apart, inject reactants onto the furnace). The jet visible on Fig. 3 detaches from the impinging surface at θ around 37° and then collides with a neighboring jet. Fig. 4 shows a detail of the velocity vectors in the recirculation regions formed.

Fig. 4 shows two recirculation zones: A larger one that occupies most of the θ-h/D plane represented and a smaller one near the target wall in the region of the collision of the two neighboring jets (upper right-hand corner of the plane). The collision of the two jets forms a backflow fountain with vortices induced underneath the fountain. The same flow structure was observed by Zuckerman and Lior [13] and is responsible for the enhancement of the heat transfer to the target without the hindrance of a thick developed boundary layer (see Section 4.3).

4.2. Flame characteristics

In this section, a set of contour plots show the shape of the impinging flame for the simulation with the reference parameters and the ones with the maximum and minimum values of the parameter being analyzed (other simulations were performed, but not shown). The figures present the reaction rate contours at two different planes: on the left, $x/D \in [-10, 0]$, $h/D \in [0, H/D]$ and $\theta = 0°$, and on the right, $x/D = 0$, $h/D \in [0, H/D]$ and $\theta \in [0, 45°]$. Fig. 5 illustrates the effect on the flame shape of the separation distance of the burner to the target (all parameters, except H/D, were set to the reference values (Table 1)).

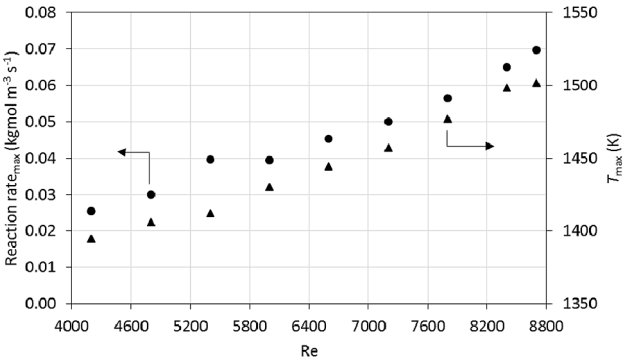

Fig. 9. Maximum reaction rate and temperature in the computational domain for propane/air flames impinging on a cylindrical surface with $D_t/D = 14.4$, $H/D = 3.5$, $\Psi = 1.8$, $T_r = 500$ K, $T_t = 850$ K.

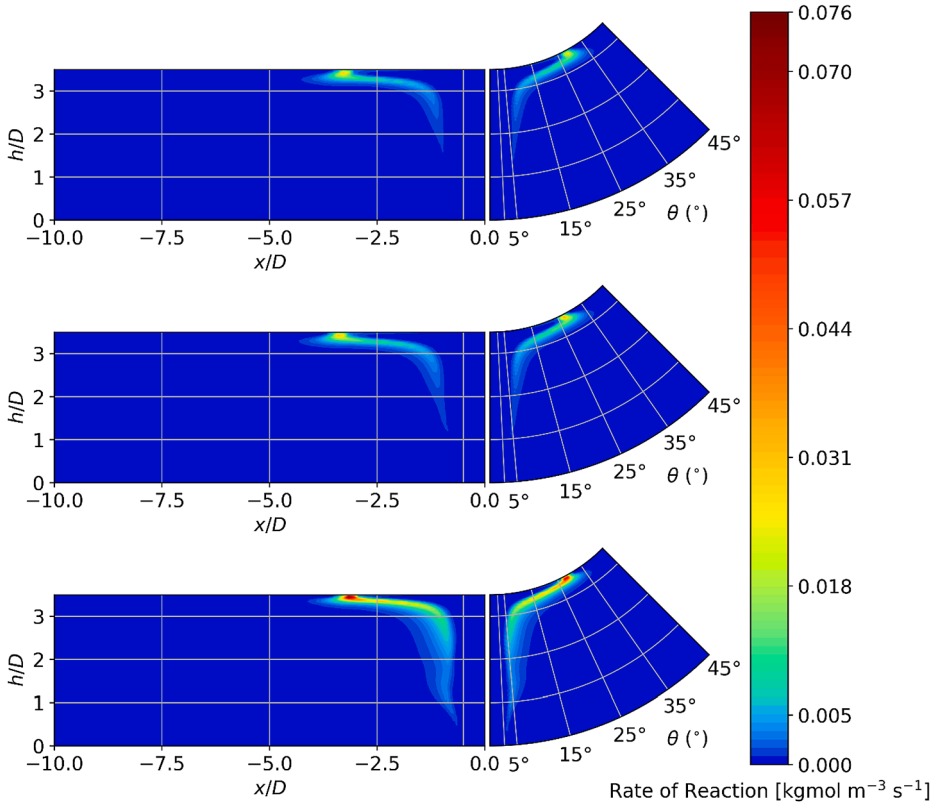

Fig. 8. Reaction rate contour plots of propane/air impinging on a cylindrical surface with $D_t/D = 14.4$, $H/D = 3.5$, $\Psi = 1.8$, $T_r = 500$ K, $T_t = 850$ K and Re equal 4200 (top), 4800 (center), and 8700 (bottom).

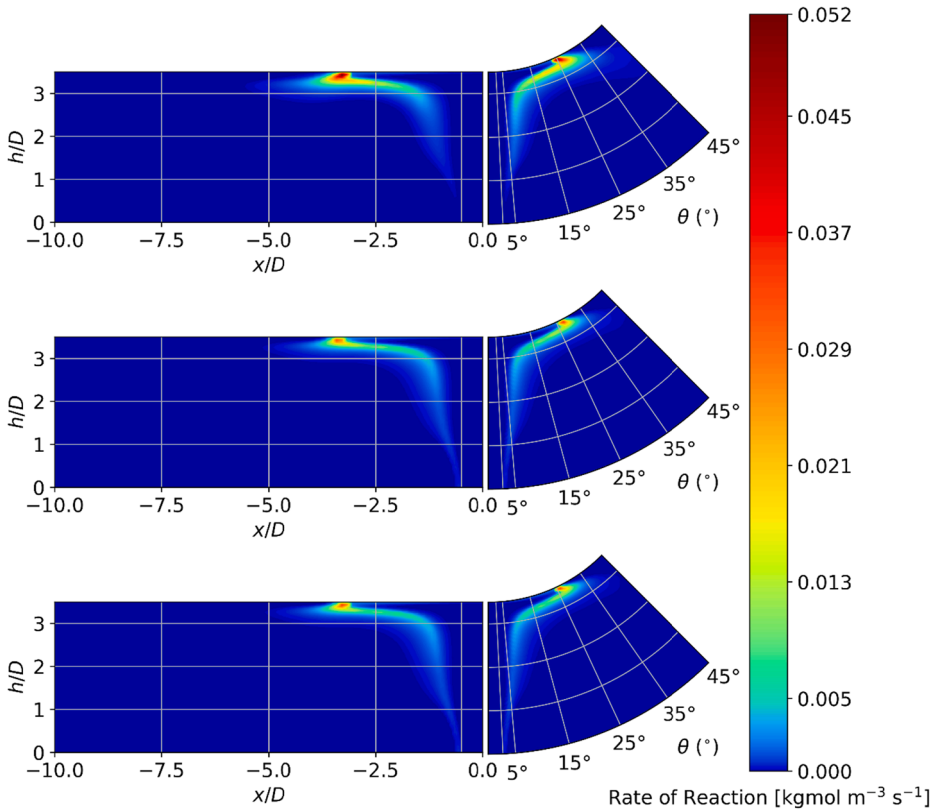

Fig. 10. Reaction rate contour plots of propane/air surfaces with $D_t/D = 14.4$, $H/D = 3.5$, Re = 4800, $T_r = 500$ K, $T_t = 850$ K, and Ψ equal to 1.0 (top), 1.8 (center) and 2.0 (bottom).

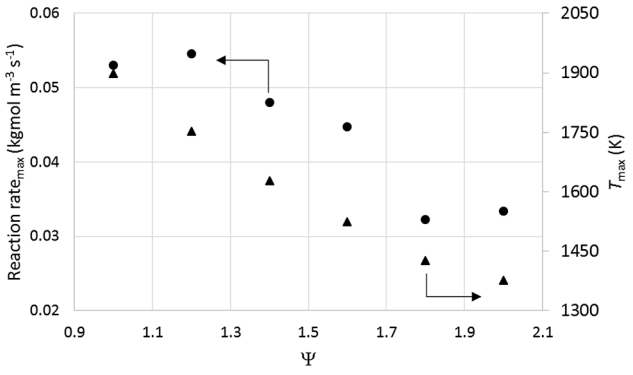

Fig. 11. Maximum reaction rate and temperature in the computational domain for propane/air flames impinging on a cylindrical surface with $D_t/D = 14.4$, $H/D = 3.5$, Re = 4800, $T_r = 500$ K, $T_t = 850$ K.

The flame shape is closely related to the proximity of the flame to the target. For a burner exit to target distance larger than the flame cone height, only hot combustion products impinge on the surface and a conical reaction zone can be observed, however, as the impinging distance is reduced, the reaction zone is intercepted by the target [5,6]. All the operating conditions analyzed in the present work, fall within the last category. For all, the colder reactants impinge directly on the target at and in the vicinity of the stagnation point and, as a consequence, flame wings are formed on the impinging surface (i.e., the chemical reactions extend to the wall jet region) and a zone of unreacted gas is present around the stagnation region (Fig. 5). This can also be observed in the temperature profiles at several heights from the burner (exemplified for the reference case in Fig. 6), which clearly show a colder core of unreacted gas from the burner exit to the target (the axis of the burner is at $x/D = 0$).

The temperature profiles at lower h/H are in the free jet region, a region with mass and momentum entrainment because of the shear-driven interaction of the burner jet and the ambient hot combustion products. Near the burner axis the temperatures are close to the colder inlet reactant temperature, but then, for $|x| > D$, sharply increase. The farther downstream, the wider the jet flame (i.e., maximum temperatures are obtained for larger $|x|/D$) and the higher the peak temperatures, which is a result of the chemical reactions occurring at the edge of the jet. Close to the target ($h = 0.95H$), the temperature profile covers both the stagnation and wall jet regions. The cooler central core of the impinging flame jet causes the area around the stagnation zone to be cooler than in the wall jet region, but hotter than the inlet reactant temperature because of heat transfer from the hot target to the reactants and energy transport within the fluid. An intense combustion zone in the wall jet region causes the temperature to rise to the peak temperature, which is significantly higher than for the other h/D.

As H/D increases, the cold reactant potential core is less perturbed by the target and the maximum temperature attained decreases. At first the maximum value of the reaction rate decreases, but then it increases. However, the differences are not large and between the lowest value of H/D considered and the highest, the relative difference in the reaction rate value is around 5%. At the lowest H/D considered, the flame wings formed are longer and the location of the maximum value of the reaction rate is generally farther from the burner axis (Fig. 7) (Both for H/D equal to 3 and 3.5, the maximum value of the reaction rate is located in a similar position at x/D and θ of 3.4 and around 27.5°, respectively, but with the increase of H/D, this location moves closer to the burner axis with x/D and θ of around 2.6 and 23.0° when H/D is 6). The reason for this is the fact that, when the target is at a larger distance from the burner exit, the deflection of the mixture that still has not reacted occurs farther downstream. If the separation distance is higher than the flame height (not simulated), all the reactants will burn before reaching the

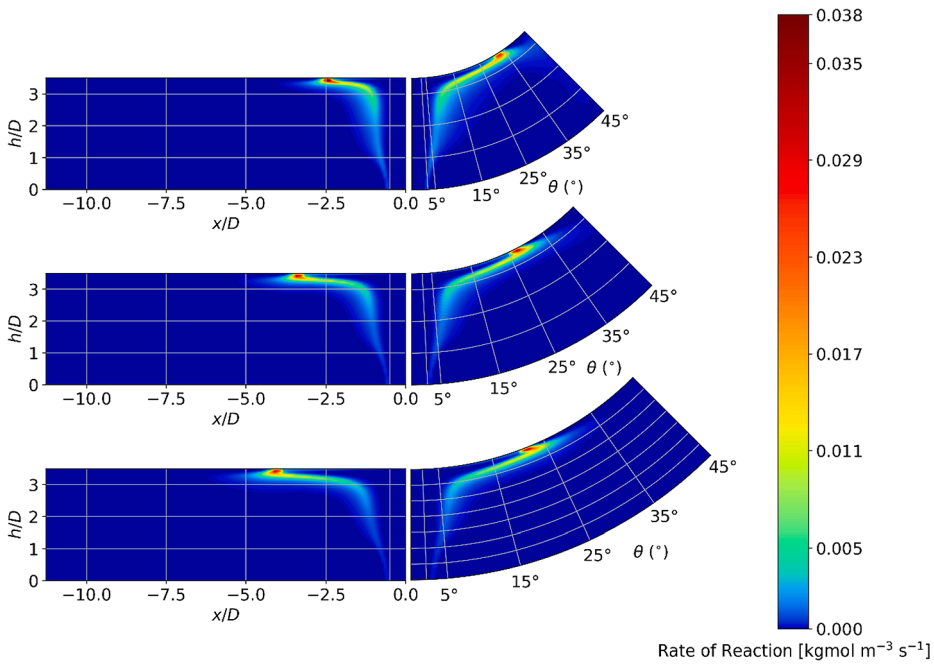

Fig. 12. Reaction rate contour plots of propane/air impinging on cylindrical surfaces with $H/D = 3.5$, Re = 4800, $\Psi = 1.8$, $T_r = 500$ K, $T_t = 850$ K, and D_t/D equal to 10 (top), 14.4 (center) and 20 (bottom).

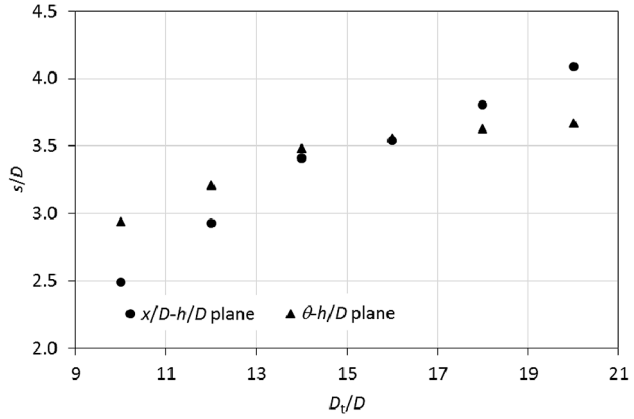

Fig. 13. Distance of the maximum reaction rate to the burner axis vs. D_t/D for propane/air flames impinging on a cylindrical surface with $H/D = 3.5$, Re = 4800, $\Psi = 1.8$, $T_r = 500$ K, $T_t = 850$ K at two different planes. At the plane x/D-h/D with $\theta = 0°$, $s/D = x/D$ and at the plane θ-h/D with $x = 0$, $s/D = \pi(D_t/2 + H\text{-}h)\theta/180$.

target and only combustion products impinge on the surface. In this case, the maximum fluid temperature near the impinging surface is located at the burner axis ($x/D = 0$) [5,6].

The behavior observed in Fig. 7 can be explained by the fact that the target is curved. After impinging perpendicularly to a flat surface, the flow is directed outward in a direction radial to the burner axis and symmetric in relation to this axis, but after impinging on a cylindrical target, the velocity vectors also present a component in the circumferential direction. The curvature causes the flow to have a larger velocity along θ than along x, which justifies the fact that the maximum reaction is farther away from the burner axis in the θ-h/D plane than in the x/D-h/D plane. This effect gets generally stronger with the increase of H/D. One possible justification is that, at larger impinging distances, the velocity gradients normal to the wall that result in the deceleration of wall jet along the circumference are smaller (because of the larger distance between the wall that confine the flow and the target, the recirculation zone is larger).

Fig. 8 illustrates the effect of the Reynolds number on the flame shape (all parameters, except Re, were set to the reference values (Table 1)). For all the Reynolds numbers analyzed, the flame impinges onto the target. As the Reynolds number increases, the velocity of the reactants at the burner exit increases, and, so does the mass flux of the premixed fuel and air mixture. This results in the increase of the reaction rate and maximum flame temperature (Fig. 9). However, more than doubling the Reynolds number has a moderate effect on the flame shape and on the location of the maximum reaction rate (between the lowest value of Re considered and the largest, the relative difference in the flame location is less than 8% for the two planes considered in Fig. 8). With a decrease in the Reynolds number, the flame is slender, the burning velocity decreases and most of the reactions move to a position closer to the target, i.e., to higher values of h/D. This is a consequence of the lower temperature gradients occurring in the fluid.

Fig. 10 illustrates the effect of the excess air ratio on the flame shape (all parameters, except Ψ, were set to the reference values (Table 1)). As in the previous cases, the flame always impinges onto the target. As expected, and shown in Fig. 11, as the excess air decreases, the reaction rate and flame temperature increase (It is well known that for hydrocarbon and air mixtures, the adiabatic flame temperature peak occurs near the stoichiometry value slightly on the rich side of the fuel [32]). As in the case of the Reynolds numbers, the flame position is not very sensitive to variations in the excess air (between stoichiometry and 100% excess air, the relative difference in the flame location is less than 5% for the two planes considered in Fig. 10). A possible explanation for this is the higher heat transfer from the fluid to the surroundings at lower excess airs.

Fig. 12 illustrates the effect of the cylinder diameter to burner diameter ratio on the flame shape. In all cases, there is flame impingement. With an increase in curvature (i.e., a decrease in D_t/D), no significant changes in the temperature of the flame occur, but the flame shape and location are altered. For the largest target diameter, the flame wings are longer (Fig. 13) and the reaction rate is lower. Most of the reaction occurs closer to target surface (consequence of the lower flame velocity and higher reactants velocity in the vicinity of the stagnation region). As $D/d \rightarrow \infty$, the flame tends towards a flame impinging on a flat

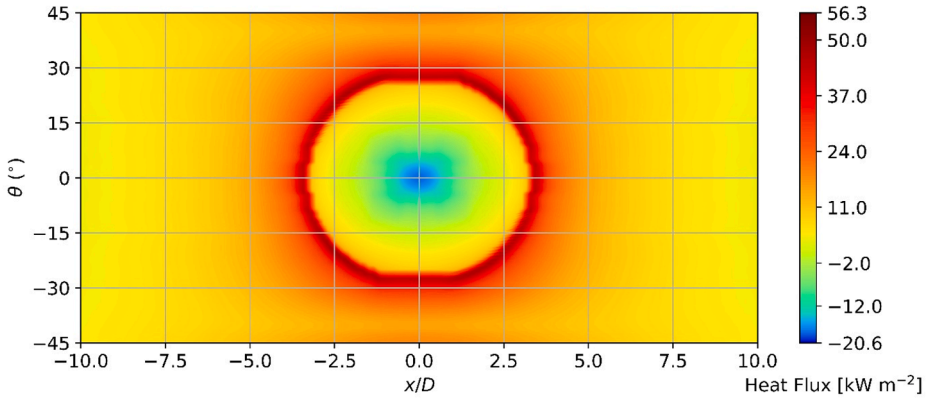

Fig. 14. Heat flux contour plot of propane/air impinging on a cylindrical surface at the target surface with D_t/D = 14.4, H/D = 3.5, Re = 4800, Ψ = 1.8, T_r = 500 K and T_t = 850 K.

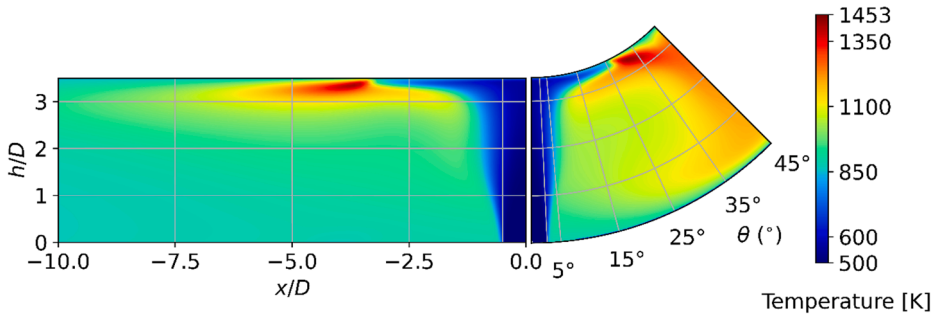

Fig. 15. Temperature field contour of propane/air impinging on a cylindrical surface at $\theta = 0^\circ$ (left) and x = 0 m (right) and with D_t/D = 13.5, H/D = 3.5, Re = 4800, Ψ = 1.8, T_r = 500 K and T_t = 850 K.

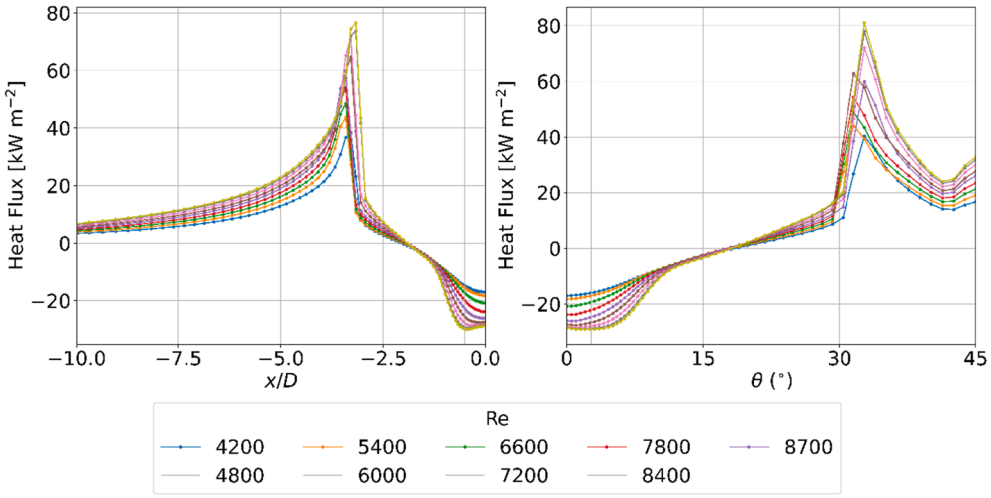

Fig. 16. Heat flux to the cylindrical target at $\theta = 0^\circ$ as a function of the axial direction (left), and x = 0 m as a function of the angular direction (right) for D_t/D = 14.4, H/D = 3.5, Ψ = 1.8, T_r = 500 K, T_t = 850 K and variable Reynolds number.

plate. One can see that, for the higher curvatures, the flame extends more in the angular direction than in the axial. However, the extension in the angular direction is limited by the adverse pressure gradient imposed by the collision with the neighboring jet. As the curvature is decreased, the flame length in both directions becomes similar and, after a certain target diameter, the flame extends more in the axial direction than in the angular one.

The effect of the reactant mixture temperature on the flame shape was also studied, but the contour plots are not shown. For all the reactant temperatures considered, the flame impinges on the target, but the consequent higher flame temperature leads to an increase in the reaction rate.

4.3. Heat flux over the target surface

Fig. 14 shows the contour plot of the heat flux from the fluid to the target for the reference condition and at the target surface ($x/D \in [-10, 10]$, $h = H$ and $\theta \in [-45^\circ, 45^\circ]$).

At the impinging region, energy is transferred from the target to the gas, because colder reactants impinge onto the surface (Fig. 15).

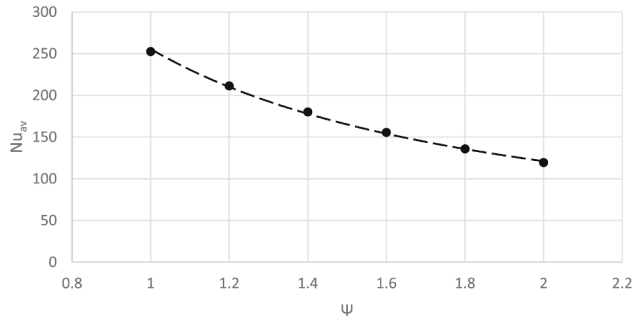

Fig. 17. Area-averaged Nusselt number as a function of the excess air ratio for $D_t/D = 14.4$, $H/D = 3.5$, Re $= 4800$, $T_r = 500$ K and $T_t = 850$ K.

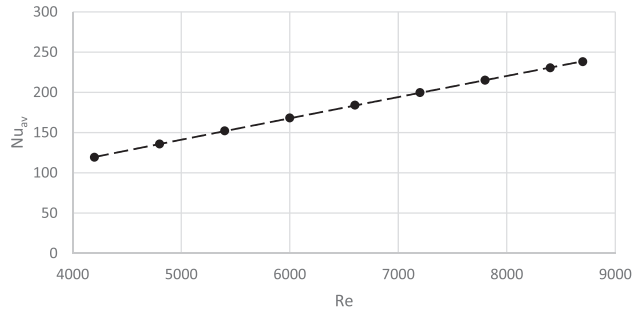

Fig. 18. Area-averaged Nusselt number as a function of the Reynolds number for $D_t/D = 14.4$, $H/D = 3.5$, $\Psi = 1.8$, $T_r = 500$ K and $T_t = 850$ K.

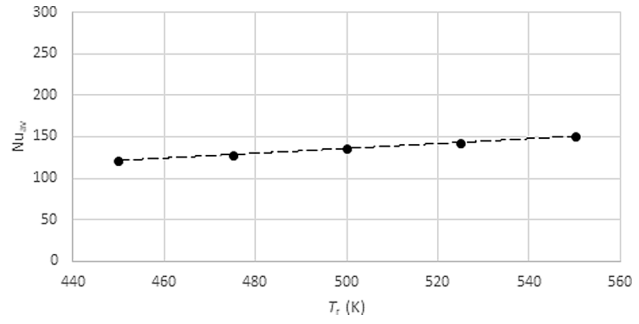

Fig. 19. Area-averaged Nusselt number as a function of the reactants temperature for $D_t/D = 14.4$, $H/D = 3.5$, Re $= 4800$, $\Psi = 1.8$ and $T_t = 850$ K.

However, as the hot products of combustion are formed in the reaction zone (Fig. 5) and enter into contact with the wall, the direction of the heat flux reverses. The maximum heat transfer occurs after the highest velocity in the wall jet region, in the vicinity of the highest temperature. In the region where the two wall jets collide ($\theta = 45^\circ$ and x in the vicinity of 0 m), the heat transfer to the target increases again because of the high turbulence existent in this region.

Fig. 16 shows the heat flux to the cylindrical target as a function of the axial direction (left) and of the angular direction (right) for several Reynolds numbers.

As described before, in the impinging region, heat is transferred from the load to the fluid because the latter is colder than the former. Combustion reactions occurring near the wall result in an increase of the fluid temperatures and, in the angular direction, at around one-sixth of the way between neighboring jets, the heat flux changes direction (i.e., heat starts being transferred to the target). This change occurs a little bit further upstream in the axial direction.

As the fluid is moving outward from the stagnation point, the heat transfer to the cylindrical surface steadily increases. In the angular direction, in the vicinity of the maximum value for the reaction rate, the gas temperatures and heat flux have a sharp increase, followed by a sharp decrease (this occurs a little bit downstream in the axial direction). After the peak, the heat flux distribution is quite different in the axial and angular directions. In the axial direction, the heat flux decreases asymptotically, while in the angular direction, there is an increase in the heat flux in the region of the separation point. This increase is explained by the collision of the two jets and the recirculation region that is formed (Fig. 4) and was also reported by Zuckerman and Lior [13], although in the case of their study, no combustion took place. Chander and Ray [5] considered impinging combustion on a circular surface of only one jet. In this case, the authors did not report an increase of the heat flux after the peak in the angular direction.

In all the cases simulated, there is flame impingement and the heat transfer to the target is enhanced by this impingement. To compare the effect of the different operation conditions on the heat transfer, the Nusselt number was averaged in the region defined by $x \in [-0.5\text{ m}, 0.5\text{ m}]$ and $\theta \in [-45^\circ, 45^\circ]$. It was observed that this non-dimensional variable increases with an increase in the Reynolds number, the ratio between the separation distance to the target and the burner diameter and the reactant temperature at the exit of the burner and decreases with an increase in the excess air ratio and the cylindrical target diameter to burner diameter ratio. The following correlation was obtained with a least-square curve fit:

$$\mathrm{Nu_{av}} = 1.96 \times 10^{-4} (D_t/D)^{-0.34} (H/D)^{0.26} (\mathrm{Re})^{0.94} (\Psi)^{-1.06} (T_r)^{1.07} \quad (10)$$

This expression is valid for confined impinging combustion on a curve wall at constant temperature, for propane and air as reactants, four radial burners, Re $\in [4200, 8700]$, $\Psi \in [1, 2]$, $H/D \in [3, 6]$, $D_t/D \in [10, 20]$ and $T_r \in [450\text{ K}, 550\text{ K}]$.

The variables that have a larger effect on the heat transfer to the target are the excess air ratio, Reynolds number and reactant temperature. However, the admissible range of variation of the latter is rather limited when compared to the other two variables. For the conditions analyzed, the excess air ratio was the dominant variable influencing the heat transfer and power required to heat the load. As the excess air ratio decreases, the fluid temperatures adjacent to the wall increase, and so do

Table A1
Parameter values considered in the simulations and area-averaged Nusselt number obtained in $x \in [-0.075\text{ m}, 0.075\text{ m}]$ and $\theta \in [-45^\circ, 45^\circ]$. The reference value case is marked in bold.

Parameter values and area-averaged Nusselt number									
Re	4200	**4800**	5400	6000	6600	7200	7800	8400	8700
$\mathrm{Nu_{av}}$	371.23	**411.05**	452.25	492.86	532.51	575.87	616.57	657.86	676.37
H/D	3	**3.5**	4	4.5	5	5.5	6		
$\mathrm{Nu_{av}}$	411.09	**411.05**	412.98	419.86	427.98	435.96	438.11		
D_t/D	10	12	**14**	16	18	20			
$\mathrm{Nu_{av}}$	516.42	475.02	**411.05**	381.51	349.81	320.04			
Ψ	1	1.2	1.4	1.6	**1.8**	2			
$\mathrm{Nu_{av}}$	787.97	675.59	569.92	485.70	**411.05**	356.87			
T_r [K]	450	475	**500**	525	550				
$\mathrm{Nu_{av}}$	341.55	379.78	**411.05**	448.29	490.13				

the temperature differences between the wall and the fluid, the heat flux to the wall and the area-averaged Nusselt number (Fig. 17). The same holds for an increase in the Reynolds number (Fig. 18) or in the temperature of the reactants at the inlet (Fig. 19). The reasons for the fluid temperature increases were explained in the previous sections.

For the range of values considered, a variation in the value of the ratio between the target diameter and the burner diameter is of secondary importance for influencing the necessary power to heat the load. As the curvature of the cylinder increases, the separation of the wall jet in the angular direction occurs earlier and the wall adjacent temperature increases due to the more intense recirculation. For the conditions analyzed, the least influential variable is the ratio between the separation distance to the target and the burner diameter. However, one should keep in mind that only cases with flame impingement were considered. If the distance between the load and the burner is higher so that the reaction zone is far from the target surface and there is only impingement of hot combustion products, it is expected that the heat flux will be affected. However, these conditions were not studied since they do not occur in the industrial furnace that served as the basis for this study.

5. Conclusions

The present paper was motivated by the lack of comprehensive studies on direct multiple flame impingement onto enclosed cylindrical targets and its importance to the understanding of the phenomena occurring inside gas-fired rapid heating furnaces. Having as a model an existent industrial furnace, a simplified geometry formed by a radial array of four burners was considered, and the reactive fluid flow and heat transfer of multiple turbulent flame jets impinging on a confined cylindrical target was simulated with the use of computational fluid dynamics. For all the operating conditions considered, the reactants impinge on the target, with the results showing the formation of flame wings and a zone of unreacted gas around the stagnation region. This causes the area around the stagnation point to be cooler and the maximum temperature to be achieved at some distance away from the stagnation point. Another important feature observed was the collision of neighboring opposed wall jets, which forms a backflow fountain with vortices induced underneath the fountain and leads to an enhancement of the local heat transfer to the load.

The present study allowed the determination of a correlation for the area-averaged Nusselt number as a function of the Reynolds number, excess air ratio, ratio between the distance of burner to target and the burner diameter, ratio between the cylindrical target diameter and burner diameter, and reactant temperature. This correlation may be used for the range of parameters simulated and shows that, under the conditions studied, the area-averaged Nusselt number is mostly influenced by the excess air ratio, the Reynolds number and temperature of reactants being also of primary importance. Optimal heat transfer to the load is obtained for stoichiometric conditions, the highest Reynolds number considered, and the highest temperature of reactants possible. Although of secondary importance, increasing the curvature of the load surface (for the same burner diameter) results in an increase in the heat transfer to the load.

CRediT authorship contribution statement

Sérgio Cavaleiro Costa: Conceptualization, Methodology, Software, Validation, Formal analysis, Data curation, Writing – review & editing, Visualization. **Isabel Malico:** Conceptualization, Methodology, Validation, Formal analysis, Resources, Writing – original draft, Writing – review & editing, Supervision, Project administration, Funding acquisition.

Declaration of Competing Interest

The authors declare that they have no known competing financial interests or personal relationships that could have appeared to influence the work reported in this paper.

Acknowledgments

The authors would like to thank Luís Rato, Paulo Canhoto, Paulo Fontes, Pedro Lima, Sofia Oliveira and Susana Cravo for the fruitful discussions.

Funding

This work was supported by the Alentejo 2020, Portugal 2020 program [Contract no. 2017/017980]; and the *Fundação para a Ciência e a Tecnologia*, through IDMEC, under LAETA [project UIDB/50022/2020]. The funding sources had no involvement in study design; in the collection, analysis and interpretation of data; in the writing of the report; and in the decision to submit the article for publication.

Appendix

In each set of simulation, one of the five parameters chosen was modified, while the others were set to the reference value (see Table 1 or values in bold in Table A1). Table A1 presents the values of the parameters that were changed in each simulation and the averaged Nusselt number obtained in the region defined by $x \in [-0.075\ \text{m}, 0.075\ \text{m}]$ and $\theta \in [-45^{\circ}, 45^{\circ}]$. These results complement the ones presented in the main body of the paper.

References

[1] G.K. Malikov, D.L. Lobanov, K.Y. Malikov, V.G. Lisienko, R. Viskanta, A. G. Fedorov, Direct flame impingement heating for rapid thermal materials processing, Int. J. Heat Mass Transf. 44 (9) (2001) 1751–1758.

[2] G. Malikov, V. Lisienko, Y. Malikov, J. Wagner, H. Kurek, Y. Chudnovsky, R. Viskanta, Mathematical modeling of direct flame impingement heat transfer, in: ASME International Mechanical Engineering Congress and Exposition, vol. 47845, 2006, pp. 615–623.

[3] P. Kuntikana, S.V. Prabhu, Heat transfer investigations on impinging flame jets of a multi-port convex burner, Appl. Therm. Eng. 142 (2018) 793–814.

[4] P.O. Oketch, M. Gonchikzhapov, U. Bergmann, B. Atakan, Thermographic phosphor heat flux measurements of laminar methane/air flame impinging on a cylindrical surface, Meas. Sci. Technol. 30 (9) (2019) 094003, https://doi.org/10.1088/1361-6501/ab217e.

[5] S. Chander, A. Ray, Heat transfer characteristics of laminar methane/air flame impinging normal to a cylindrical surface, Exp. Therm Fluid Sci. 32 (2) (2007) 707–721.

[6] V. Yousefi-Asli, E. Houshfar, F. Beygi-Khosroshahi, M. Ashjaee, Experimental investigation on temperature field and heat transfer distribution of a slot burner methane/air flame impinging on a curved surface, Appl. Therm. Eng. 129 (2018) 761–771.

[7] P.O. Oketch, U. Bergmann, B. Atakan, CH4/air-flame impingement heat transfer to a cylindrical surface. Joint meeting of the German and Italian Sections of the Combustion Institute, 23–26 May, Sorrento, Italy, 2018.

[8] P. Kuntikana, S.V. Prabhu, Heat transfer investigations on methane-air premixed flame jet exiting from a circular nozzle and impinging over semi-cylindrical surfaces, Int. J. Therm. Sci. 128 (2018) 105–123.

[9] G.K. Hargrave, M. Fairweather, J.K. Kilham, Forced convective heat transfer from premixed flames—Part 2: Impingement heat transfer, Int. J. Heat Fluid Flow 8 (2) (1987) 132–138.

[10] H.S. Zhen, L. Zhang, Z.L. Wei, Z.B. Chen, Z.H. Huang, A numerical study of the heat transfer of an impinging round-jet methane Bunsen flame, Fuel 251 (2019) 730–738.

[11] R. Viskanta, Heat transfer to impinging isothermal gas and flame jets, Exp. Therm Fluid Sci. 6 (2) (1993) 111–134.

[12] K. Rönnberg, C. Duwig, Heat transfer and associated coherent structures of a single impinging jet from a round nozzle, Int. J. Heat Mass Transf. 173 (2021) 121197, https://doi.org/10.1016/j.ijheatmasstransfer.2021.121197.
[13] N. Zuckerman, N. Lior, Radial slot jet impingement flow and heat transfer on a cylindrical target, J. Thermophys. Heat Transfer 21 (3) (2007) 548–561.
[14] X.L. Wang, J.H. Lee, T.J. Lu, S.J. Song, T. Kim, A comparative study of single-/two-jet crossflow heat transfer on a circular cylinder, Int. J. Heat Mass Transf. 78 (2014) 588–598.
[15] S. Pachpute, B. Premachandran, Effect of number of round jets on impingement heat transfer from a heated cylinder, Appl. Therm. Eng. 162 (2019) 114308, https://doi.org/10.1016/j.applthermaleng.2019.114308.
[16] S. Pachpute, B. Premachandran, Turbulent multi-jet impingement cooling of a heated circular cylinder, Int. J. Therm. Sci. 148 (2020) 106167, https://doi.org/10.1016/j.ijthermalsci.2019.106167.
[17] L.L. Dong, C.W. Leung, C.S. Cheung, Heat transfer of a row of three butane/air flame jets impinging on a flat plate, Int. J. Heat Mass Transf. 46 (1) (2003) 113–125.
[18] L.C. Kwok, C.W. Leung, C.S. Cheung, Heat transfer characteristics of an array of impinging pre-mixed slot flame jets, Int. J. Heat Mass Transf. 48 (9) (2005) 1727–1738.
[19] S. Chander, A. Ray, Heat transfer characteristics of three interacting methane/air flame jets impinging on a flat surface, Int. J. Heat Mass Transf. 50 (3-4) (2007) 640–653.
[20] H. Shariatmadar, A. Momeni, A. Karimi, M. Ashjaee, Heat transfer characteristics of laminar slot jet arrays impinging on a constant target surface temperature, Appl. Therm. Eng. 76 (2015) 252–260.
[21] Z.H. Lin, Y.J. Chou, Y.H. Hung, Heat transfer behaviors of a confined slot jet impingement, Int. J. Heat Mass Transf. 40 (5) (1997) 1095–1107.
[22] D.H. Lee, S.J. Kim, Y.H. Kim, H.J. Park, Heat transfer with fully developed slot jets impinging on confined concave and convex surfaces, Int. J. Heat Mass Transf. 88 (2015) 218–223.
[23] Y.H. Kim, D.H. Lee, S.H. Han, Investigation of impingement surface geometry effects on heat transfer in a laminar confined impinging slot jet, Int. J. Heat Mass Transf. 115 (2017) 347–353.
[24] D. Höser, P.h. Rudolf von Rohr, Experimental heat transfer study of confined flame jet impinging on a flat surface, Exp. Therm Fluid Sci. 91 (2018) 166–174.
[25] S.C. Costa, I. Malico, R.P.M. Lima, L. Rato, Numerical simulation of a large-scale industrial billet heating furnace with direct flame impingement, Defect Diffus. Forum 407 (2021) 11–21.
[26] T.H. Shih, W.W. Liou, A. Shabbir, Z. Yang, J. Zhu, A new k-ε eddy viscosity model for high Reynolds number turbulent flows, Comput. Fluids 24 (3) (1995) 227–238.
[27] B.F. Magnussen, B.H. Hjertager, On mathematical models of turbulent combustion with special emphasis on soot formation and combustion, in: 16th Symp. (Int'l.) on Combustion, The Combustion Institute, 1976.
[28] ANSYS, FLUENT software. https://www.ansys.com/products/fluids/ansys-fluent (Last access on 2019.08.02).
[29] J.P. Vandoormaal, G.D. Raithby, Enhancements of the SIMPLE method for predicting incompressible fluid flows, Numer. Heat Transfer 7 (1984) 147–163.
[30] G.D. Raithby, E.H. Chui, A Finite-Volume Method for predicting a radiant heat transfer in enclosures with participating media, J. Heat Transfer 112 (1990) 415–423.
[31] E.H. Chui, G.D. Raithby, Computation of radiant heat transfer on a nonorthogonal mesh using the finite-volume method, Numer. Heat Transfer 23 (3) (1993) 269–288.
[32] C. Law, A. Makino, T. Lu, On the off-stoichiometric peaking of adiabatic flame temperature, Combust. Flame 145 (4) (2006) 808–819.